

Article

Mapping Groundwater Prospective Areas Using Remote Sensing and GIS-Based Data Driven Frequency Ratio Techniques and Detecting Land Cover Changes in the Yellow River Basin, China

Shuhang Li ¹, Mohamed Abdelkareem ^{2,*}  and Nassir Al-Arifi ³¹ Ural Institution, North China University of Water Resources and Electric Power, Zhengzhou 450045, China² Geology Department, South Valley University, Qena 83523, Egypt³ Chair of Natural Hazards and Mineral Resources, Geology and Geophysics Department, King Saud University, Riyadh 68953, Saudi Arabia

* Correspondence: mohamed.abdelkareem@sci.svu.edu.eg

Abstract: Groundwater is an essential resource that meets all of humanity's daily water demands, supports industrial development, influences agricultural output, and maintains ecological equilibrium. Remote sensing data can predict the location of potential water resources. The current study was conducted in China's Yellow River region, Ningxia Hui Autonomous Region (NHAR). Through the use of a GIS-based frequency ratio machine learning technique, nine layers of evidence influenced by remote sensing data were generated and integrated. The layers used are soil characteristics, aspect, and roughness index of the terrain, drainage density, elevation, lineament density, depressions, rainfall, and distance to the river from the location. Six groundwater prospective zones (GWPZs) were found to have very low (13%), low (30%), moderate (25%), high (16%), very high (11%), and extreme potentiality (5.26%) values. According to well data used to validate the GWPZs map, approximately 40% of the wells are consistent to very high to excellent zones. Information about groundwater productivity was gathered from 150 well locations. Using well data that had not been used for model training, the resulting GWPZs maps were validated using area-under-the-curve (AUC) analysis. FR models have an accuracy rating of 0.759. Landsat data were used to characterize the study area's changes in land cover. The spatiotemporal differences in land cover are detected and quantified using multi-temporal images which revealed changes in water, agricultural, and anthropogenic activities. Overall, combining different data sets through a GIS can reveal the promising areas of water resources that aid planners and managers.

Keywords: groundwater; remote sensing; GIS; data-driven modeling

Citation: Li, S.; Abdelkareem, M.; Al-Arifi, N. Mapping Groundwater Prospective Areas Using Remote Sensing and GIS-Based Data Driven Frequency Ratio Techniques and Detecting Land Cover Changes in the Yellow River Basin, China. *Land* **2023**, *12*, 771. <https://doi.org/10.3390/land12040771>

Academic Editor: Paolo Nasta

Received: 20 February 2023

Revised: 20 March 2023

Accepted: 22 March 2023

Published: 29 March 2023



Copyright: © 2023 by the authors. Licensee MDPI, Basel, Switzerland. This article is an open access article distributed under the terms and conditions of the Creative Commons Attribution (CC BY) license (<https://creativecommons.org/licenses/by/4.0/>).

1. Introduction

The ability to access water is crucial for maintaining life. Since the beginning of the twenty-first century ref. [1], population growth, environmental, climatic, and socio-economic variables have all contributed to an increasing worry about the demand for fresh water in the world. Water resources are necessary for the growth of the agricultural, urban, and industrial sectors. In terms of total freshwater resources, groundwater makes up around 20% of them, placing it behind glaciers and lakes which make up only 1% and 79%, respectively, of the world's total freshwater resources. It is one of the water reserves that can be used to combat the problem of water shortage [2,3] as it can be used when necessary and is an effective substitute for limited surface water, which is getting harder to find [1]. Groundwater is increasingly needed around the world for a variety of reasons [4,5] because it is more predictable and fresher than surface water, less likely to be polluted, always present, widely accessible, has great natural quality, is clean and accessible, and is inexpensive [6]. It is crucial to remember that 80% of the world's rural population relies

on groundwater for their clean drinking water. It is an essential water resource since it provides drinking water to more than half of the population [7].

Because groundwater resources are buried beneath strata, it is vital to use prediction models to investigate and uncover water resources [8–10] utilizing various methods. Groundwater discovery by traditional means is more time- and money-consuming. Groundwater exploration, prediction, and regional estimation can be done using remote sensing (RS) and geographic information systems (GIS) [11,12]. A GIS technique can be used to combine and interpret large amounts of geographical data to forecast and locate new water sources [13]. The RS and GIS can be used to identify potential groundwater resource locations, as demonstrated by several studies [9,14,15]. For instance, multi-criteria decision-making is a quick and economical method [5,10].

In groundwater modeling, several knowledge-based (overlay, AHP, Boolean logic, index overlays, and analytical hierarchy process) and data-driven (e.g., WOE, machine learning models, logistic regression, weights of evidence, linear regression decision tree analysis, and neural networks) techniques are frequently used [16,17]. The frequency ratio (FR) approach, a data-driven and bivariate statistical method, assesses spatial relationships between the dependent variable, e.g., water wells, and the independent variables, namely classes of thematic layers, to assign a rating (r) rate to each factor [18,19]. It is widely applied in probabilistic processes such as geohazards [20–23] and in groundwater exploration in different environments [3,24–31]. The FR method provided better results than the evidential belief function (EBF) method [16,32] and gave valuable information when coupled with the overlay analysis. In this technique, several criteria such as geologic, topographic, climatic, and hydrologic information are utilized for the prediction of groundwater occurrences by preparing, normalizing, and combining these elements [33].

The permeability and porosity of aquifer elements are influenced by soil parameters [34] and soil geometry, as the existence of sand and gravel deposits boosts porosity, which is an important factor in recharging groundwater aquifers [35]. This is due to the runoff of water through time-induced soil erosion [36,37]. When they flow in the same direction, elevation significantly affects groundwater penetration and motion [38–40] as runoff lowers groundwater potential in elevated regions, which also lowers the capacity for recharging [41]. Additionally, the vegetation has gotten bigger on the faces to the north and east that promote the recharging of groundwater. Geomorphologic characteristics such as TRI have garnered a lot of interest, since it is essential for groundwater transport and management in any research region. Moreover, with increasing distance from rivers, the likelihood of encountering groundwater decreases [38,42]. The hydrologic element of rainfall (R_f) is a significant source of recharge [43,44]. Precipitation has a significant impact on percolation and recharging.

The LU/LC changes require thorough research in order to be properly planned, utilized, and regulated for challenging environmental studies. Researchers can assess and monitor the dynamics of natural resources using the LU/LC by utilizing remote sensing techniques, which are crucial for sustainable management. In addition, the LU/LC offers crucial evidence of the availability of water supplies. The present study aims to apply the GIS-based hydride FR and weighted overlay technique for optimization and revealing promising areas for water resources through analysis of multi-factors derived from satellite data/images.

2. Study Area

The Yellow River, Ningxia Hui Autonomous Area, in central China is the location of the current study (Figure 1). It covers a region with coordinates of $35^{\circ}45'43.30''$ and $35^{\circ}58'20.83''$ N and longitudes of $105^{\circ}8'18.82''$ and $107^{\circ}16'31.3''$ E. It covers about 35,915 km². Oriented from north to south, it drains the Yellow River basin. The Ningxia Hui Autonomous Area in northwest China is the area under investigation [45]. It is situated in the area of the inner desert. Warm continental arid and semi-arid weather and adequate light energy are present at the study site. The average annual sunlight hours are expected to

range from 2194 to 3082; the mean annual temperature will be between 5 and 9 degrees Celsius; and the average annual precipitation ranges from 200 to 680 mm, with most of the precipitation occurring in the summer. Groundwater may be divided into two groups: the northern area's water and the southern area's water of the Quaternary deposits, depending on hydrodynamic characteristics, aquifer types, and occurrence parameters of groundwater karst in the southern area [46,47].

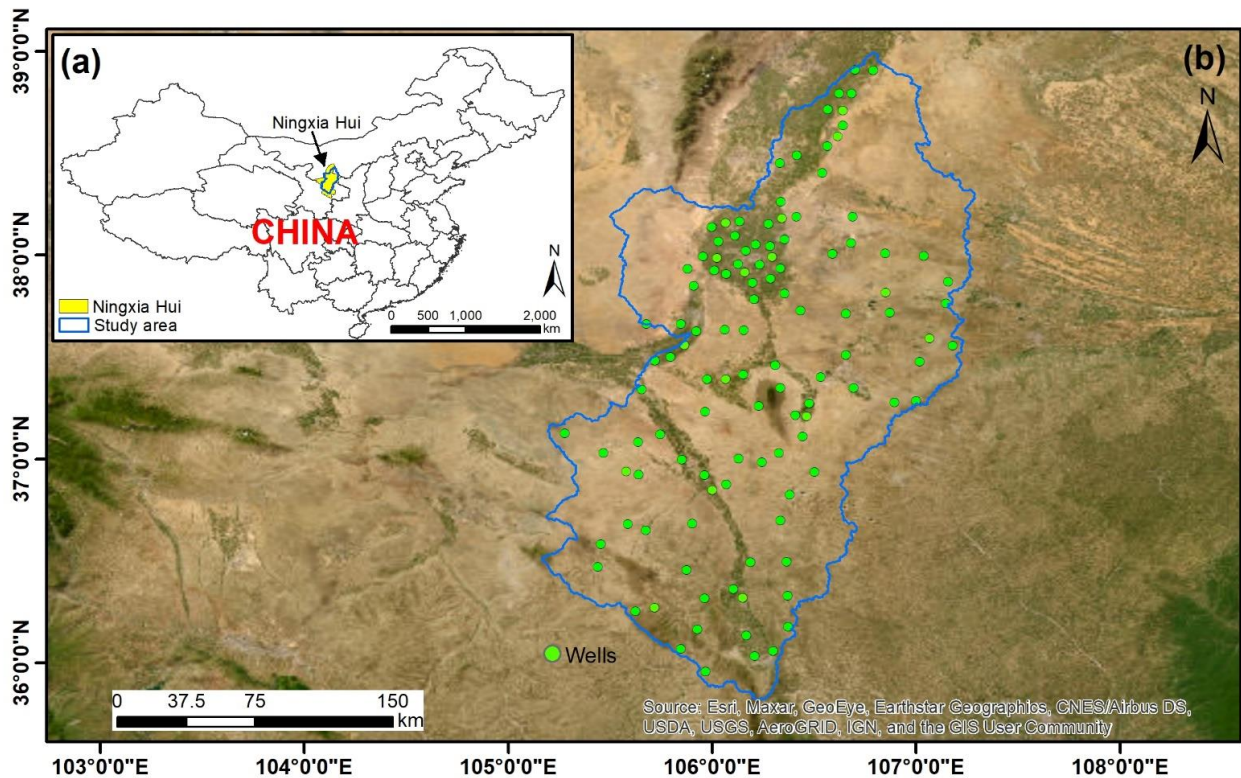


Figure 1. (a) Location map of the present study area is marked in the blue polygon that covers the majority of Niangxia Hui Region; (b) watershed of the study area overlain by well data.

3. Data and Methods

This study combined topography, hydrologic, and meteorological data with remote sensing information from several sensors to show potential water resource areas. GIS methods were utilized to combine various thematic maps created from these data, including those of the soil, elevation, aspect, terrain roughness index, depression, lineaments, drainage density, distance to a river, and rainfall intensity (Figure 2).

The DEMs were derived from the SRTM data (90 m cell size) of NASADEM 1arc second WGS84 data (NASADEM 1arc second WGS84). The stream network was generated by the 8D approach [48], and the stream density map was produced via a GIS program. Estimating the depressions to illustrate where water accumulates can similarly be done using the “fill-difference” method [10]. The OLI and TIRS sensors are carried by Landsat 8, which was launched on 11 February 2013. To map the land use and cover, VNIR and SWIR wavelength regions are used. Here, mosaiced obtained sceneries that featured the OLI bands 2, 3, 4, 5, and 7 underwent image alterations and enhancing procedures. Landsat-8 data “LC08_L1TP_129034_20220312_20220312_02_RT” was utilized to display vegetation and the signature of water resources.

4. Results

4.1. Soil

Due to geometric characteristics and the nature of the soil of the surface layer regulating how much precipitation seeps into the subsurface aquifer, lithological parameters are crucial. The size, shape, and arrangement of the soil grains, as well as the pore system that corresponds to them, can all have a major impact on the vertical and lateral flow of water. The development and management of groundwater resources depend mostly on the soil. Based on the arrangement of soil grains controlling the infiltration and recharge, each soil type was given a set of soil and textural characteristics based on the SWAT Soil Data classes for the various category levels in soil classification. The soil map of the study area is divided into Calcic xerosols (loam), Luvisc xerosols (sandy clay loam), Lithosols (loam), Eutric Gleysols (clay loam), and Calcic cambisols (loam), which account for 26.13, 0.66, 53.06, 19.29, and 0.87% of the total area, respectively (Figure 3a).

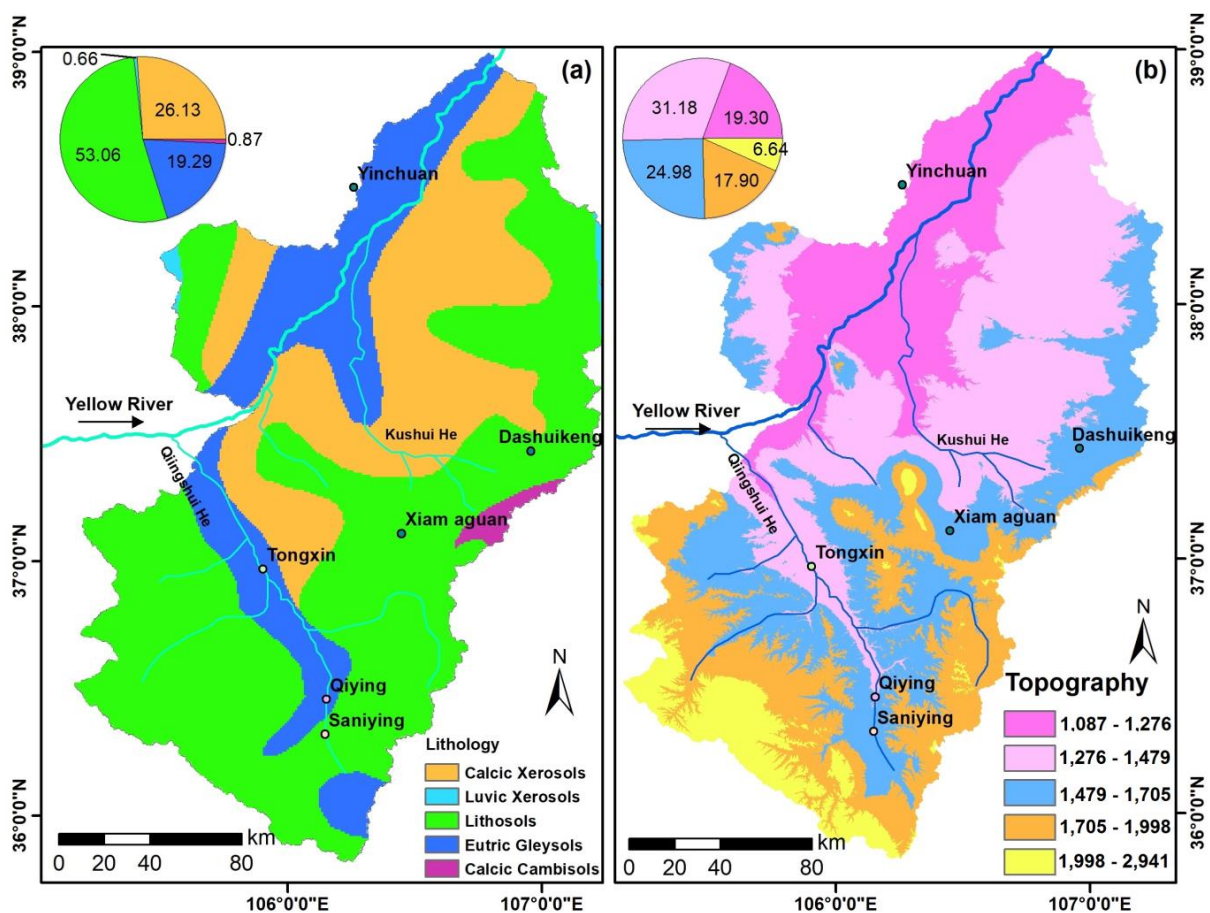


Figure 3. (a) Soil map of the study area; (b) Digital elevation model (DEM) data of the present study displays the variations in elevation.

4.2. Elevation

The flow of groundwater and surface discharge is influenced by topography. The link between infiltration and low-altitude areas is positive. Considering this, it is likely that low-lying places accumulate surface water following severe storms that drain downstream networks. Due to the substantial infiltration of river water, groundwater potential is often high in plain floodplain zones but decreases at high elevations. The topographical layer is crucial in determining groundwater availability, recharge capacity, and water movement across the land [4]. Therefore, the elevation map of the study region varies from 1087 to 2941 m. The elevation map (Figure 3b) was divided into three classes, 1087 to 1276, 1276 to

1479, 1479 to 1705, and 1705 to 1998, encompassing 19, 31, 25, 18, and 7% of the total area, respectively.

4.3. Aspects

The DEM in ArcGIS 10.8 is used to extract aspects. There are 10 categories for aspect measurements: flat (or no aspect direction), N, NE, E, SE, S, SW, W, and NW. Water resources are more prevalent north of the Earth’s equator on slopes that look north and east than on slopes that stand facing south and west. The mountain’s eastern and northern slopes get less sunlight than its southern and western sides. The aspect map (Figure 3b) which was derived from the DEM was divided into three categories: Flat (-1), N (0–22.5), NE, E, SE, S, SW, W, NW, and N. These categories, collectively account for 0.26, 8.45, 14.54, 10.98, 10.29, 12.08, 12.92, 11.29, and 12.

4.4. Topography Roughness Index (TRI)

The TRI, a geomorphometric index that identifies and quantifies the geometry of land-surface terrain in the area under investigation, has an impact on groundwater occurrence as well. Afterward, using ArcGIS and the Natural Break Classifier (NBC), the TRI map was separated into four classes. The TRI map (Figure 4b) was divided into five categories: 0.614 to 0.889, 0.535 to 0.614, 0.461 to 0.535, 0.379 to 0.461, and 0.111 to 0.379 which, respectively, covered 10, 24, 31, and 10% of the overall region.

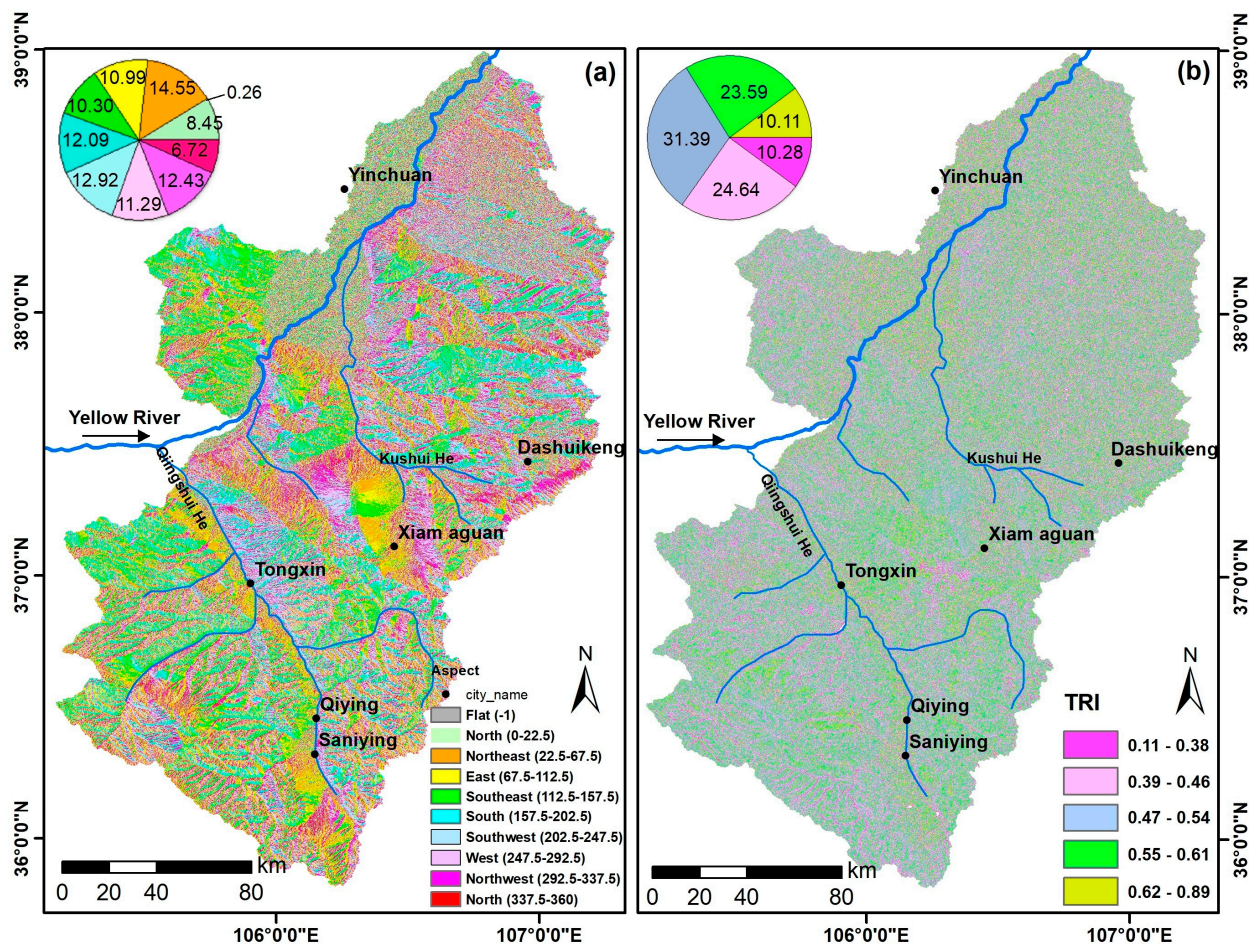


Figure 4. (a) Aspect map of the study area; (b) Terrain roughness index of the present study.

4.5. Depressions/Sinks

Areas with low surface elevations that might be flooded during rainstorms are indicated by topographic depressions. These depressions can be filled with precipitated water until the water level increases to the point where the flow can exit. These areas are suitable for water resources because they flood the low topography. ArcMap version 10.5's spatial analysis can identify depressions using SRTM DEMs. The research region's 95.8, 2.7, and 1.5% of the depression map (Figure 5a) were categorized into three classes: 0–1, 1–3.8, and 3.8–72 (Table 1).

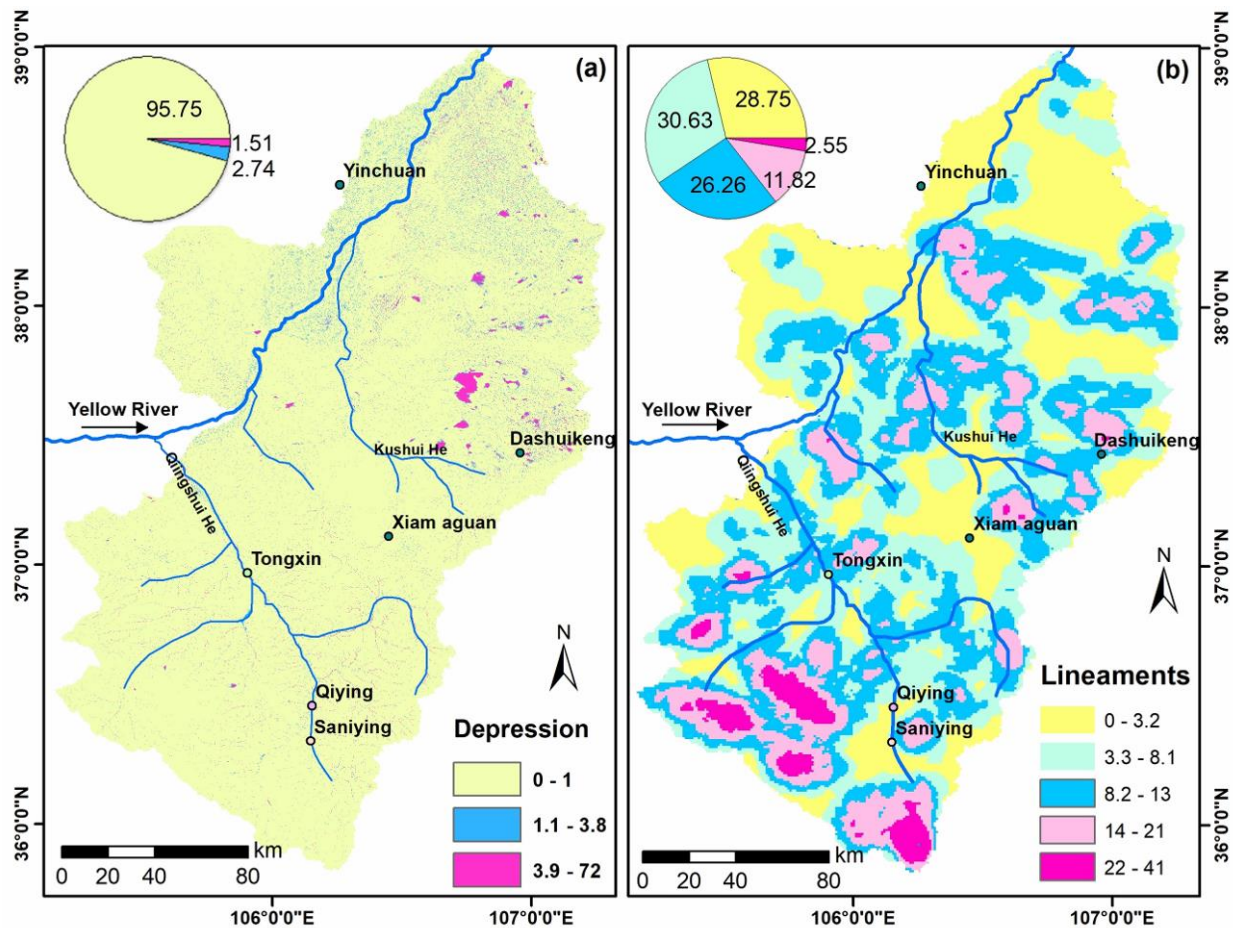


Figure 5. (a) Topographic depression map of the study area; (b) lineaments of the present study.

Table 1. Factors controlling groundwater prospectivity.

Elevation	No. Pixels in Domain	Domain %	No. Wells	No. Wells %	FR
1087 to 1276	1,016,102	0.19	38	0.38	1.97
1276 to 1479	1,641,795	0.31	20	0.2	0.64
1479 to 1705	1,315,398	0.25	24	0.24	0.96
1705 to 1998	942,575	0.18	15	0.15	0.84
1998 to 2941	349,645	0.07	3	0.03	0.45
TRI classes					
0.614 to 0.889	542,030	0.10	12	0.12	1.17
0.535 to 0.614	1,244,420	0.24	21	0.21	0.89
0.461 to 0.535	1,655,667	0.31	27	0.27	0.86

Table 1. *Cont.*

Elevation	No. Pixels in Domain	Domain %	No. Wells	No. Wells %	FR
0.379 to 0.461	1,299,650	0.25	24	0.24	0.97
0.111 to 0.379	533,086	0.10	16	0.16	1.58
Dd reclasses					
5.31 to 31.10	6537	0.12	6	0.06	0.49
31.20 to 43.10	15,167	0.29	26	0.26	0.91
43.20 to 54.30	15,598	0.29	30	0.3	1.02
54.40 to 66.70	11,203	0.21	24	0.24	1.14
66.80 to 101	4551	0.09	14	0.14	1.63
Soil					
Calcic xerosols	13,224	0.261334	21	0.21	0.80
Luvic xerosols	332	0.006561	0	0	0.00
Lithosols	26,848	0.530572	35	0.35	0.66
Eutric Gleysols	9759	0.192858	43	0.43	2.23
Calcic cambisols	439	0.008676	1	0.01	1.15
Dist River					
1480 to 1750	1,870,410	0.046373	0	0	0
1110 to 1480	5,139,914	0.127435	12	0.12	0.94
740 to 1110	8,467,401	0.209934	13	0.13	0.62
370 to 740	11,778,792	0.292033	32	0.32	1.10
0 to 370	13,077,205	0.324225	43	0.43	1.33
Depression					
0 to 1	5,041,843	0.957521	95	0.95	0.99
1 to 3.8	144,133	0.027373	4	0.04	1.46
3.8 to 72	79,539	0.015106	1	0.01	0.66
ASPECT					
Flat (−1)	13,758	0.002613	0	0	0
North (0–22.5)	444,969	0.084506	20	0.2	2.37
Northeast (22.5–67.5)	766,094	0.145493	20	0.2	1.37
East (67.5–112.5)	578,467	0.10986	4	0.04	0.36
Southeast (112.5–157.5)	542,320	0.102995	6	0.06	0.58
South (157.5–202.5)	636,523	0.120885	11	0.11	0.91

Table 1. *Cont.*

Elevation	No. Pixels in Domain	Domain %	No. Wells	No. Wells %	FR
Southwest (202.5–247.5)	680,426	0.129223	9	0.09	0.70
West (247.5–292.5)	594,492	0.112903	12	0.12	1.06
Northwest (292.5–337.5)	654,449	0.12429	13	0.13	1.05
North (337.5–360)	354,017	0.067233	5	0.05	0.74
Lineaments					
0 to 3.3	14,814	0.29	34	0.34	1.18
3.3 to 8.04	15,780	0.31	30	0.3	0.98
8.04 to 13.30	13,530	0.26	23	0.23	0.88
13.30 to 21.10	6090	0.12	10	0.1	0.85
21.10 to 40.87	1312	0.03	3	0.03	1.18
Precipitation					
234 to 288	4585	0.28	34	0.34	1.21
288 to 338	4168	0.26	26	0.26	1.01
338 to 394	4408	0.27	25	0.25	0.92
394 to 477	3094	0.19	15	0.15	0.79

4.6. Lineaments

Lineaments are linear geometrical structures that represent underlying cracks in the earth's surface [51]. These structures can be used to better define the existing aquifers and discover new reservoirs near densely populated areas that promote fluid migration to the bottom [52] and lineaments that can provide information on water penetration and circulation [53]. When compared to other topographical features, they are the porosity of secondary sources and are visible as textural changes on satellite photos. A lineament might be anything from a crack to a fracture to a master joint. Long, linear geological formations, topographic linearity, and the straight routes that streams follow are further examples [54]. They affect how deeply runoff water permeates below the strata and replenishes the aquifer's groundwater flow and storage. The lineament density map (Figure 5b) was obtained after digitizing lineaments from satellite images and then classified using Natural Breaks intervals into five classes, viz., 0 to 3.3, 3.3 to 8.04, 8.04 to 13.30, 13.30 to 21.10, and 21.10 to 40.87, covering 29, 31, 26, 12, and 3 % of the study area (Table 1; Figure 5b).

4.7. Distance to River

Alluvial deposits are typically found in river channels, especially in semi-arid regions; therefore, being close to hydrological systems is important when looking for water resources. The ideal circumstances for excellent penetration and, consequently, groundwater replenishment are provided by neighboring rivers. Utilizing data on rivers that were gathered from the OSM dataset, the distance from rivers was determined using ArcGIS' "Euclidean distance function". Spatial Analyst Tools were used to determine the distance from the river, which was then divided into five categories (Figure 6a): 1480 to 1750, 1110 to 1480, 740 to 1110, 370 to 740, and 0 to 370. These categories, which covered 4.64, 12.74, 20.99, 29.20, and 32.42 percent of the total area, respectively, each represented a different distance from the river.

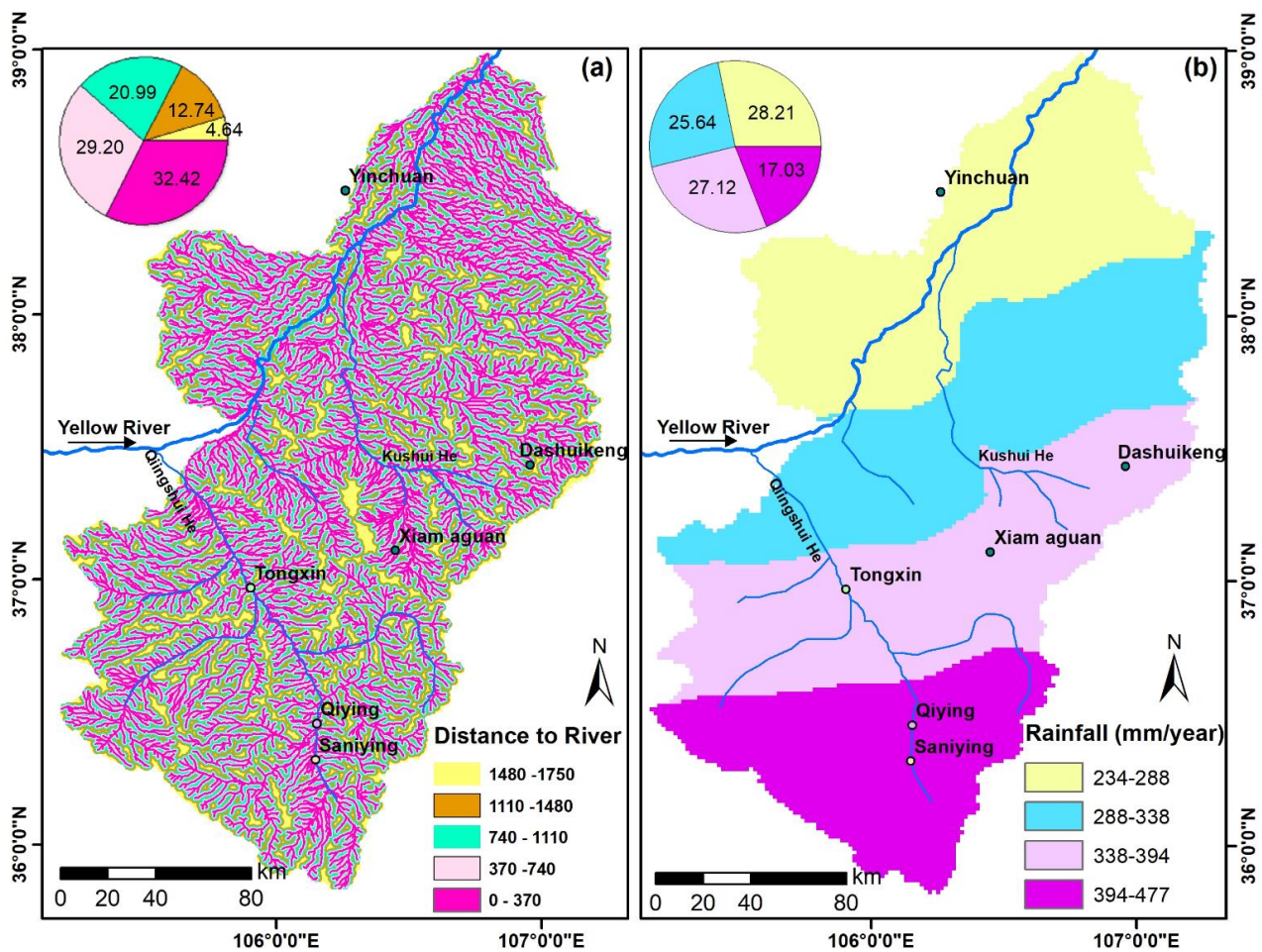


Figure 6. (a) Distance to river map of the study area; (b) rainfall of the present study.

4.8. Rainfall Data

The distribution and volume of rainfall determine how much water is present in a hydrologic system. Rainfall intensity in a region allows for surface water accumulation which promotes infiltration, recharging, and runoff. The frequent precipitation through the years is the main source of rivers, lakes, and recharging the groundwater aquifers [26,55]. Because rainfall is the main source of recharging the groundwater aquifers through the years, it is essential for this process [56,57].

The area that is exposed to storms that bring rain encourages groundwater recharge when it rains. Researchers can monitor, document, and measure the frequency of rainstorms in the watershed under study using information from the CRU data. Due to the high precipitation and flooding caused by this downpour, there was a scarcity of water supply, and infrastructure was severely damaged.

The study area’s yearly mean rainfall from 2011 to 2020 was provided by the Climate Research Unit (<https://crudata.uea.ac.uk/cru/data/hrg/> accessed on 10 January 2022). The precipitation point format was modified into a raster format using Multidimensional Tools of Spatial Analyst. We next converted the raster format to points by the Conversion Tools [49], which were interpolated by applying the Kriging method.

The rainfall map was classified into four classes, viz., 234 to 288, 288 to 338, 338 to 394, and 394 to 477 covered 28, 26, 27, and 19 % of the study area, respectively (Figure 6b).

4.9. Drainage Density (Dd)

Drainage density, which is an effective indication for predicting infiltration rates, controls the relationship between water flow and water penetration in a terrain [58]. By dividing the total number of streams and rivers in a drainage basin by its surface area, the drainage density of that basin can be determined [58,59]. The kind of vegetation, the soil’s ability to absorb precipitation, the slope gradient, and the bedrock nature and structure all have an impact on where rainfalls [1]. Locations with less surface runoff and high drainage density have higher infiltration rates. A zone with high groundwater capacity is indicated by high drainage density values because they favor runoff [10]. The Dd map (Figure 7a,b) was divided into four classes, encompassing 12, 29, 29, and 9% of the area, respectively, from 5.31 to 31.10, 31.20 to 43.10, 43.20 to 54.30, and 54.40 to 66.70.

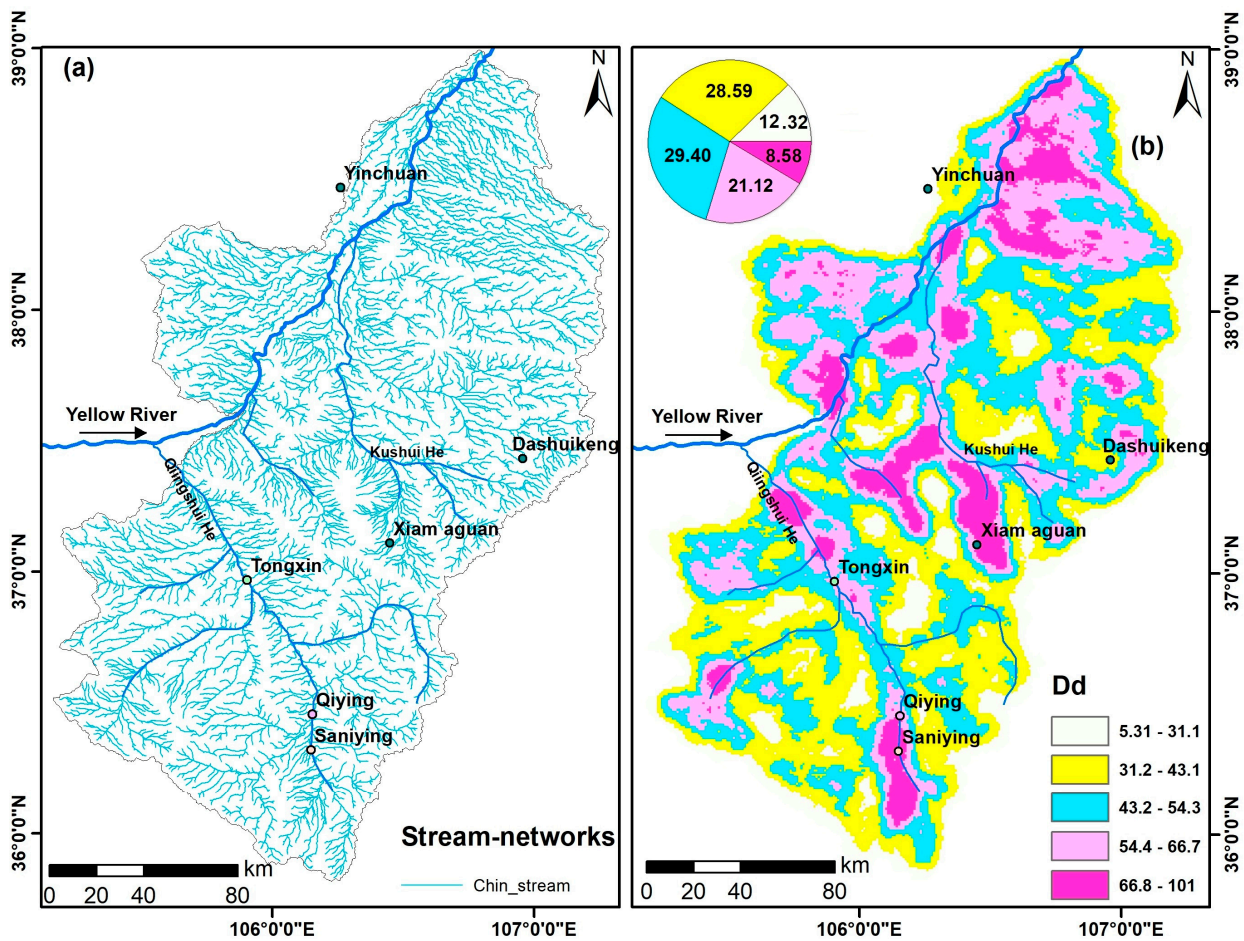


Figure 7. (a) Stream-networks of the study area; (b) drainage density of the present study.

5. Groundwater Potential Mapping and Validation of the Built Models

FR is the possibility that a phenomenon matches a given feature. [13]. The locations of the validated wells and the training variables (the independent variables), e.g., the soil, and Dd were entered using the FR method [60]. The frequency of wells in each class for all parameters was determined using FR [13]. Using the below formula (Equation (2)), it was determined how each factor affected the predictor:

$$FR = (A/B)/(C/D) \tag{2}$$

A represents the percentage of points in each class, B is the total number of points across all classes, C is the number of classes, and D is the total number of pixels, where FR seems to be the ratio at which each class of each feature affects the parameter. The weights of each class of factors associated with the subject layers for delineating GWPZs are determined by the FR values generated for each class of conditioning factors. The new thematic layer is the input value to the hybrid model after each class has been subjected to FR.

In order to ascertain the spatial correlations between well sites and training factors, the FR model was applied (Table 1). FR values below 1 denote low correlation, while those above 1 denote higher correlation [61]. The greatest FR (1.97) was recorded for elevation classes (Figure 8) 1087 to 1276, followed by 1479 to 1705 (0.96), 1705 to 1998 (0.84), 1276 to 1479 (0.64), and 1998 to 2941. (0.45). As a result, regions with low elevations between 1087 and 1276 are more likely to contain groundwater. Additionally, the range from 1 to 3.8 (FR = 1.46) has the largest potentiality in the context of depressions, while the ranges from 0 to 1 (FR = 0.99) and 3.8 to 72 (FR = 0.66) have low potentialities.

The lowest FR (1.21) for rainfall classes (Figure 8) was found in locations receiving between 234 and 288 mm, followed by 288 and 338 mm (1.01). The lowest FR values were found in areas with a lot of precipitation: 338 to 394 mm (0.92) and 394 to 477 mm (0.79).

The soils classed as Eutric Gleysols “clay loam” (FR 2.23) and Calcic cambisols “loam” (FR 1.15) have FR values, while Luvic xerosols “sandy clay loam” (FR = 0) is the lowest and has no potential.

The class of TRI with the highest probability of groundwater potential was 0.111 to 0.379 (FR = 1.58), followed by 0.614 to 0.889 (FR = 1.17) and 0.379 to 0.461 (FR = 0.97). The TRI classes of 0.461 to 0.535 (FR = 0.86) and 0.535 to 0.614 (FR = 0.89) have low probability. The slope aspect group with the highest FR (2.37) belongs to N (0–22.5), followed by NE (1.37), west (1.06), and NW (1.05). While Flat (−1) has little potential, other characteristics such as E (0.36), SE (0.58), SW (0.70), N (337.5–360) (0.74), and S (0.91) are at their lowest. The categories from 0 to 370 m (FR= 1.33) and 370 to 740 m (FR = 1.10) had the highest probabilities for places in terms of their proximity to rivers. The potential is zero for 1110 to 1480 (FR = 0.94), 740 to 1110 (FR = 0.62), and 1480 to 1750 (FR = 0).

High potentiality occurs mostly in the Dd ranges of 66.80 to 101 (FR = 1.63), 54.40 to 66.70 (FR = 1.14), and 43.20 to 54.30 (FR = 1.02) in terms of drainage density. The groundwater potentiality is low in the lower instances of the drainage density ranging from 5.31 to 31.10 (FR= 0.49) and 31.20 to 43.10 (FR= 0.91), respectively. High potentiality can be seen in the lineament density of low values 0 to 3.3 (FR = 1.18) and high values 21.10 to 40.87 (FR = 1.18). The other classes were 3.3 to 8.04, 8.04 to 13.30, and 13.30 to 21.10 (FR = 0.98, 0.88, and 0.85, respectively).

The integrated groundwater potential zone (GWPZ) map, which was created by combining nine thematic maps, was then divided into six classes using a natural break approach, ranging from extremely low to high potentiality (Figure 9a). The classes considered were very low (13.13%), low (29.97%), moderate (25.07%), high (16.01%), very high (10.56%), and extremely high potentiality (5.26%) (Figures 8 and 9a). The majority of the extremely high to extreme GWPZ is covered by plant and water resources, according to Landsat-8 band composites 7, 5, and 3 (Figure 9b–d).

The ROC curve for GWPZ is shown in Figure 10. The AUC emphasizes the importance of the prediction by demonstrating the system’s capacity to predict “groundwater” and “no-existence of groundwater” with equal accuracy. The AUC is a 0-to-1 scale which scores less than 0.5, suggesting model coherence and higher simulations have greater accuracy. The results demonstrate great accuracy in creating a groundwater potential map by fusing statistical models with the RF model. The improved accuracy of the model (AUC = 0.759) is caused by the results’ unknown existence of groundwater.

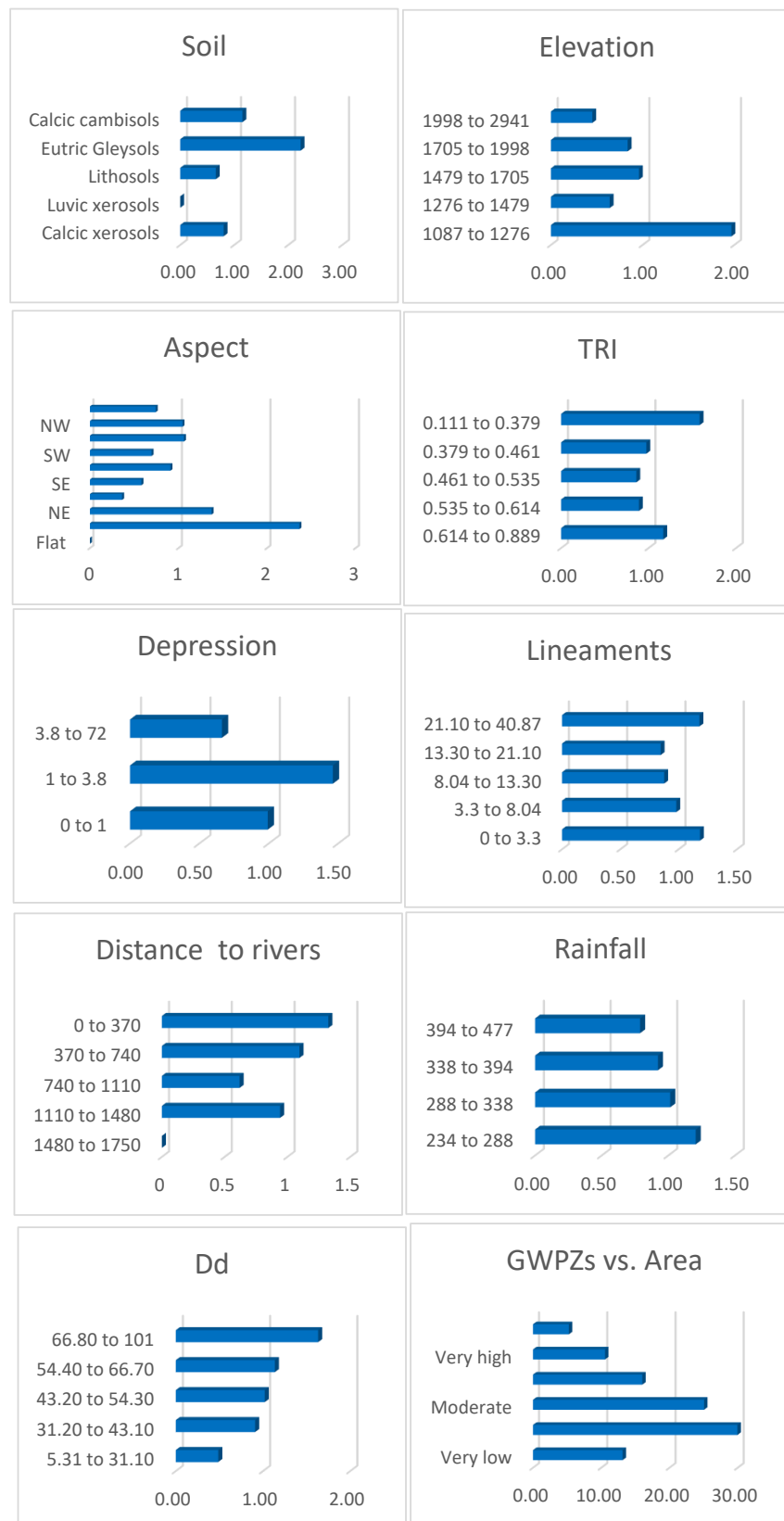


Figure 8. A two-dimensional bar chart, for comparing the FR values among classes of the influencing factors (e.g., soil, elevation, aspect, TRI, depressions, lineaments, distance to rivers, rainfall, and drainage density (Dd)) and the areas covering the GWPZs.

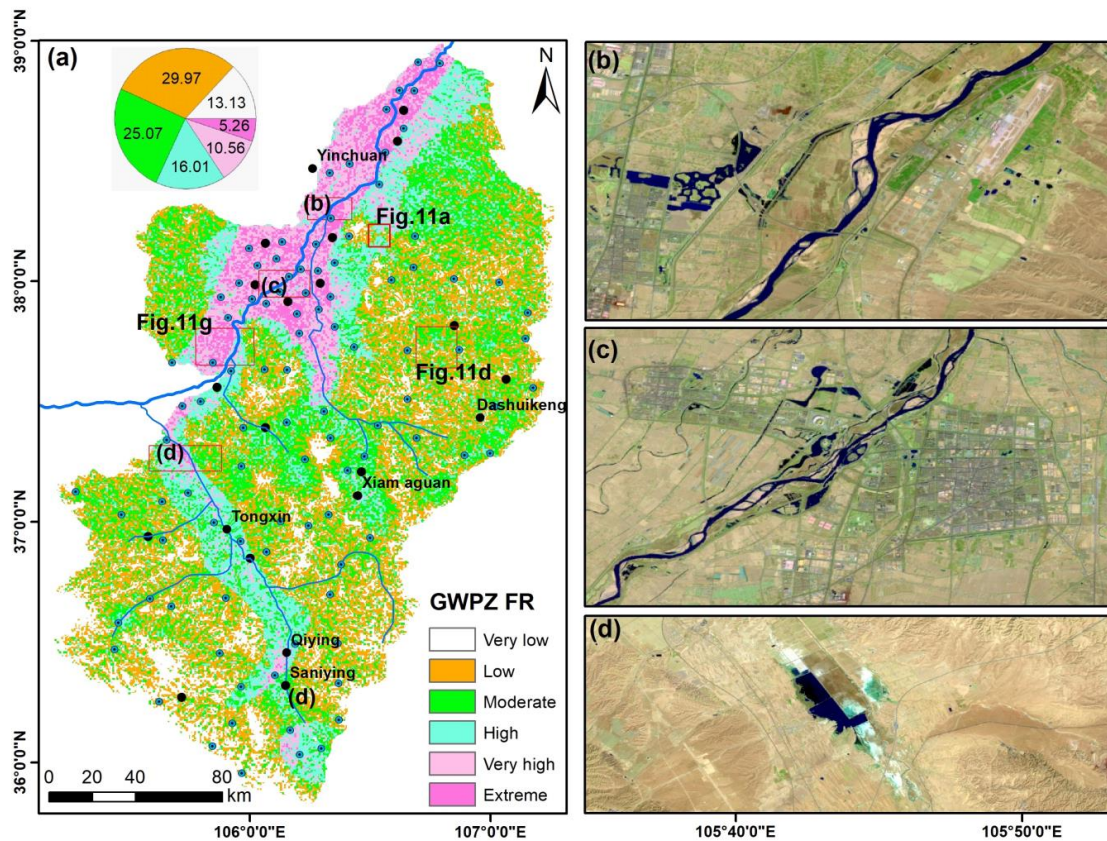


Figure 9. (a) Groundwater prospective map of the study area; (b–d) Subsets of Landsat 753 band composites display the vegetation in green and water in dark blue color.

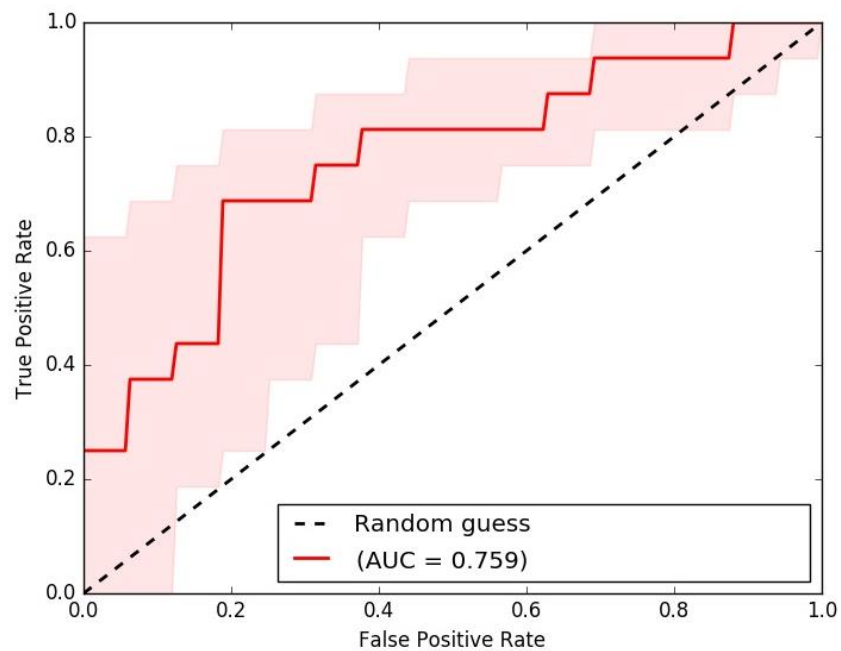


Figure 10. Model validation of GWPZ map.

6. Changes Detection of in Land Use Land Cover

The analyses of land use and land cover (LULC) have the capacity to identify water resources that increase the quantity of agriculture and other anthropogenic activities [62]. In order to plan, use, and regulate natural resources effectively for complicated environmental

studies, LULC changes must be well studied. Through the use of remote sensing techniques, which are extremely essential for sustainable management, researchers are able to evaluate and track the dynamics of natural resources using the LULC [63,64]. Additionally, the LULC provides important proof of the provision of water supplies.

Differences between two Landsat images acquired on 23/2/2010 (Landsat-5; bands 7, 4, and 2 in R, G, and B) and 12/3/2022 (Landsat-8; 7, 5, and 3 in R, G, and B) are assessed using the Difference tool of ArcGIS. To quantify the changes in LULC, the “Difference” function in ArcGIS is utilized. The differences between Landsat images from 2010 and 2022 are quantified (Figure 11). In this approach, the zero value reflects coherence among the processed images, and the more change between the multi-temporal images the farther the value divergence from zero. In Figure 11a,d,g, the differences in land cover/land use between Landsat 2010 and 2022 are detected in blue (positive); however, negative changes appear in dark brown. Such an approach detected changes in water, vegetation, and infrastructures. Based on this approach, the area experienced major changes regarding anthropogenic activities. There were more abundances of water in 2022 lakes than in 2010 as shown in Figure 11d–f, and more land reclamation in Figure 11h versus Figure 11g. The analyses of land use and land cover have the capacity to identify water resources that increase the quantity of agriculture and other anthropogenic activities.

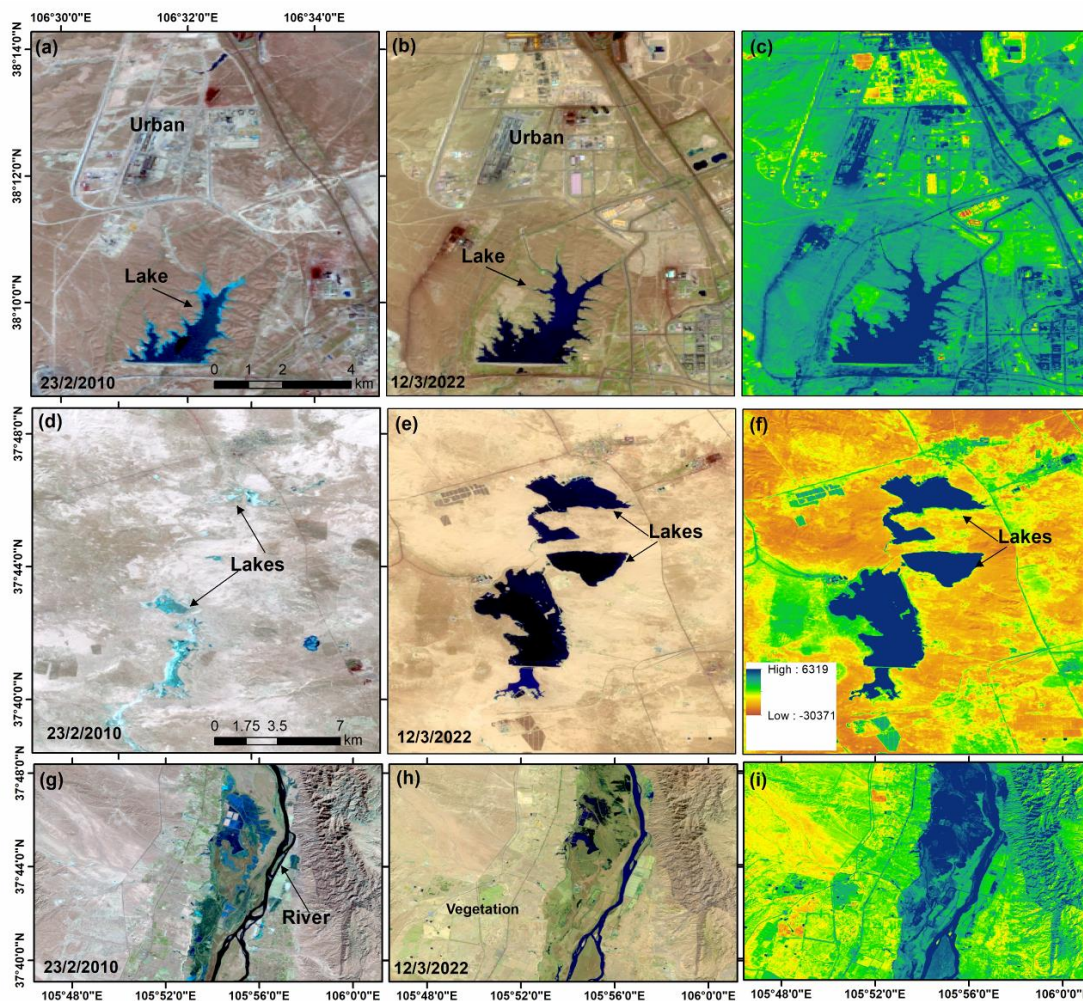


Figure 11. Landsat data (a,d,g) Landsat-5 band composite 7, 4, and 2; (b,e,h) Landsat OLI 7, 5, and 3; (c,f,i) differences in land cover in years 2010 and 2022.

7. Discussion

Based on the analysis of hydrologic, geologic, topographic, and climatic data, the downstream area has high groundwater potentiality as indicated by the spatial and statistical analysis of the input factors. The soil of “clay loam” and Calcic cambisols “loam” recorded high FR values are 2.23 and 1.15, respectively. This is because the rate of precipitation and groundwater infiltration is substantially controlled by the soil characteristics [49,65], as the arrangement of soil grains controlled the infiltration and recharge capability and has a major impact on the vertical and lateral flow of water [66]. Additionally, porous and permeable rocks facilitate water infiltration by subsurface fluxes [52]. The existence of an equal proportion of sand, silt, and clay of lithosols facilitates the recharge potential due to watershed and soil erosion (Nguyen et al., 2021). Therefore, the amount and flow of groundwater in a specific area are determined by the soil underneath that location [67]. Because the surface water can accumulate and drain downstream networks [4,68], the low-elevation areas recorded the highest FR (1.97) for elevation classes 1087 to 1276. Based on FR values, the N and NE have higher values of 2.37 and 1.37, respectively, increasing the vegetation in some areas which improves surface infiltration and groundwater recharge [11,69]. On hillsides that look north and east, transpiration is low despite the significant soil moisture levels. The TRI factor was computed to assess how heterogeneous the landscape was, and it was utilized to search for groundwater [63,64]. The areas of low TRI have a high FR value of 1.58 and are positively related to water accumulation. The groundwater aquifers would be able to receive water at topographic depressions [10,16], as they recorded high FR values of 1.46 and 0.66. Furthermore, high lineament density areas have a high FR value of 1.18. This is due to that location with high permeability and potential groundwater [67,70–72] and, thus, groundwater occurrence. Geologic structures, such as drainage networks (rivers) and geological features (faults, fractures, and lithological limits), are rectilinear due to a phenomenon that takes place below the surface of the ground [52]. Such structures increase secondary porosity and infiltration. The areas “0–370” km, as they are nearby rivers, are considered the more pronounced groundwater [64,73], as being close to hydrological systems is important when looking for water resources [5,52]. The rainfall information may be useful in identifying regions that are likely to accumulate water and represent the potential recharge areas [9,10,49,56]. Although the areas of high rainfall has the lowest FR value (0.79), the area with low rainfall has the highest FR (1.21) as the precipitation is driven by topography but water accumulates in low elevated areas in rugged terrains [74]. Based on that Dd, classes 54.40 to 66.70 and 66.80 to 101 have the higher values 1.63 and 1.14. This is because the areas dissected by lineaments have higher Dd. It suggests that high-drainage-density locations are suited for the formation of groundwater [75–78]. In similar studies concerning groundwater prospection which implemented bivariate statistical models [3,25,74], it was found that the present study provided more balanced results for the training and validation points. Although the present study presented a satisfactory output and validation performance, the results are controlled by the quality of input data. Moreover, detailed field investigations and very high-resolution images that reflect the hydrogeologic and geologic settings should be utilized to predict the groundwater potentiality in the future.

8. Conclusions

In this article, a part of the Yellow River basin that covers 35,915 km² was investigated to delineate the prospective locations of water resources. To achieve that, geological, hydrologic, topographic, and climatic data were combined with remote sensing and GIS data. Nine predictive GIS maps including soil, elevation, lineaments, rainfall intensity, Dd, Distance to the river, TRI, aspect, and topographic data were prepared and normalized using the FR technique, which ranked each sub-class based on its capability for holding groundwater. These layers were integrated using the overlay weight-based GIS technique. The resulting map was then classified using NBC into six groundwater prospection zones were found to have very low (~13%), low (~30%), moderate (~25%), high (~16%), very

high (~11%), and extreme potentiality (~5.26%) of the entire area. The most plausible place for groundwater resources is downstream. In conclusion, taking into account GWPZ's investigation is beneficial for research field decision-makers who are considering long-term sustainability.

Author Contributions: Conceptualization, M.A.; methodology, M.A.; software, M.A.; validation, S.L.; investigation, M.A.; resources, N.A.-A.; writing—original draft preparation, M.A., S.L. and N.A.-A.; writing—review and editing, M.A., S.L. and N.A.-A. All authors have read and agreed to the published version of the manuscript.

Funding: This research received no external funding.

Data Availability Statement: Not applicable.

Acknowledgments: Nassir Al-Arifi extends his grateful to the Deanship of Scientific Research, King Saud University for funding through the Vice Deanship of Scientific Research Chairs.

Conflicts of Interest: The authors declare that they have no conflict of interest.

References

1. Abd Manap, M.A.; Sulaiman, W.N.A.; Ramli, M.F.; Pradhan, B.; Surip, N. A knowledge-driven GIS modeling technique for groundwater potential mapping at the Upper Langat Basin, Malaysia. *Arab. J. Geosci.* **2013**, *6*, 1621–1637. [[CrossRef](#)]
2. Carmon, N.; Shamir, U. Water-sensitive planning: Integrating water considerations into urban and regional planning. *Water Environ. J.* **2010**, *24*, 181–191. [[CrossRef](#)]
3. Jaafarzadeh, M.S.; Tahmasebipour, N.; Haghizadeh, A.; Pourghasemi, H.R.; Rouhani, H. Groundwater recharge potential zonation using an ensemble of machine learning and bivariate statistical models. *Sci. Rep.* **2021**, *11*, 5587. [[CrossRef](#)] [[PubMed](#)]
4. Mallick, J.; Khan, R.A.; Ahmed, M.; Alqadhi, S.D.; Alsubih, M.; Falqi, I.; Hasan, M.A. Modeling Groundwater Potential Zone in a Semi-Arid Region of Aseer Using Fuzzy-AHP and Geoinformation Techniques. *Water* **2019**, *11*, 2656. [[CrossRef](#)]
5. Sun, T.; Cheng, W.; Abdelkareem, M.; Al-Arifi, N. Mapping Prospective Areas of Water Resources and Monitoring Land Use/Land Cover Changes in an Arid Region Using Remote Sensing and GIS Techniques. *Water* **2022**, *14*, 2435. [[CrossRef](#)]
6. Jha, M.K.; Bongane, G.M.; Chowdary, V.M. Groundwater potential zoning by remote sensing, GIS and MCDM techniques: A case study of eastern India. In Proceedings of the Symposium JS.4 at the IAHS and IAH convention, Hyderabad, India, 6–12 September 2009; IAHS Press: Wallingford, UK, 2009; pp. 432–441.
7. Ramachandra, T.V. *Soil and Groundwater Pollution from Agricultural Activities*; Commonwealth of Learning: Vancouver, BC, Canada; Center for Ecological Science, Indian Institute of Science: Karnataka, India; TERI Press: New Delhi, India, 2006; p. 352.
8. Abdelkareem, M.; El-Baz, F. Analyses of optical images and radar data reveal structural features and predict groundwater accumulations in the central Eastern Desert of Egypt. *Arab. J. Geosci.* **2015**, *8*, 2653–2666. [[CrossRef](#)]
9. Abdelkareem, M.; Abdalla, F. Revealing potential areas of water resources using integrated remote-sensing data and GIS-based analytical hierarchy process. *Geocarto Int.* **2021**, *37*, 8672–8696. [[CrossRef](#)]
10. Zhu, Q.; Abdelkareem, M. Mapping groundwater potential zones using a knowledge-driven approach and GIS analysis. *Water* **2021**, *13*, 579. [[CrossRef](#)]
11. Arulbalaji, P.; Padmalal, D.; Sreelash, K. GIS and AHP techniques based delineation of groundwater potential zones: A case study from Southern Western Ghats. *India Sci. Rep.* **2019**, *9*, 1–17. [[CrossRef](#)]
12. Kumar, V.A.; Mondal, N.C.; Ahmed, S. Identification of groundwater potential zones using RS, GIS and AHP techniques: A case study in a part of Deccan Volcanic Province (DVP), Maharashtra, India. *J. Indian Soc. Remote Sens.* **2020**, *48*, 497–511. [[CrossRef](#)]
13. Yariyan, P.; Avand, M.; Omidvar, E.; Pham, Q.B.; Linh, N.; Tiefenbacher, J. Optimization of statistical and machine learning hybrid models for groundwater potential mapping. *Geocarto Int.* **2020**, *11*, 2282–2314. [[CrossRef](#)]
14. Abdelkareem, M.; El-Baz, F.; Askalany, M.; Akawy, A.; Ghoneim, E. Groundwater prospect map of Egypt's Qena Valley using data fusion. *Int. J. Image Data Fusion.* **2012**, *3*, 169–189. [[CrossRef](#)]
15. Hong, Y.; Abdelkareem, M. Integration of remote sensing and a GIS-based method for revealing prone areas to flood hazards and predicting optimum areas of groundwater resources. *Arab. J. Geosci.* **2022**, *15*, 1–14. [[CrossRef](#)]
16. Abdelkareem, M.; Abdalla, F.; Al-Arifi, N.; Bamousa, A.O.; El-Baz, F. Using remote sensing and GIS-based frequency ratio technique for revealing groundwater prospective areas at Wadi Al Hamdh watershed, Saudi Arabia. *Water* **2023**, *15*, 1154. [[CrossRef](#)]
17. Pradhan, A.; Nair, A.; Indu, J.; Kirstetter, P.-E. Impact of Sampling of GPM Orbital Data on Streamflow Simulations. *J. Hydrol.* **2020**, *593*, 125798. [[CrossRef](#)]
18. Naghibi, S.A.; Pourghasemi, H.R.; Dixon, B. GIS-based groundwater potential mapping using boosted regression tree, classification and regression tree, and random forest machine learning models in Iran. *Environ. Monit. Assess.* **2016**, *188*, 44. [[CrossRef](#)]

19. Arshad, A.; Zhang, Z.; Zhang, W.; Dilawar, A. Mapping favorable groundwater potential recharge zones using a GIS-based analytical hierarchical process and probability frequency ratio model: A case study from an agro-urban region of Pakistan. *Geosci. Front.* **2020**, *11*, 1805–1819. [[CrossRef](#)]
20. Fan, H.; Lu, Y.; Hu, Y.; Fang, J.; Lv, C.; Xu, C.; Feng, X.; Liu, Y. A Landslide Susceptibility Evaluation of Highway Disasters Based on the Frequency Ratio Coupling Model. *Sustainability* **2022**, *14*, 7740. [[CrossRef](#)]
21. Lee, S.; Pradhan, B. Landslide hazard mapping at Selangor, Malaysia using frequency ratio and logistic regression models. *Landslides* **2007**, *4*, 33–41. [[CrossRef](#)]
22. Pradhan, B. Landslide susceptibility mapping of a catchment area using frequency ratio, fuzzy logic and multivariate logistic regression approaches. *J. Indian Soc. Remote Sens.* **2010**, *38*, 301–320. [[CrossRef](#)]
23. Regmi, A.D.; Yoshida, K.; Pradhan, B.; Pourghasemi, H.R.; Khumamoto, T.; Akgun, A. Application of frequency ratio, statistical index and weights-of-evidence models, and their comparison in landslide susceptibility mapping in Central Nepal Himalaya. *Arab. J. Geosci.* **2013**, *7*, 725–742. [[CrossRef](#)]
24. Nampak, H.; Pradhan, B.; Manap, M.A. Application of GIS based data driven evidential belief function model to predict groundwater potential zonation. *J. Hydrol.* **2014**, *513*, 283–300. [[CrossRef](#)]
25. Razandi, Y.; Pourghasemi, H.Z.; NajmehSamaniNeisani, N.S.; Rahmati, O. Application of analytical hierarchy process, frequency ratio, and certainty factor models for groundwater potential mapping using GIS. *Earth Sci. Inform.* **2015**, *8*, 867–883. [[CrossRef](#)]
26. Guru, B.; Seshan, K.; Bera, S. Frequency ratio model for groundwater potential mapping and its sustainable management in cold desert, India. *J. King Saud Univ. Sci.* **2017**, *29*, 333–347. [[CrossRef](#)]
27. Neshat, A.; Pradhan, B. An integrated DRASTIC model using frequency ratio and two new hybrid methods for groundwater vulnerability assessment. *Nat. Hazards* **2015**, *76*, 543–563. [[CrossRef](#)]
28. Ahmadi, H.; Kaya, O.A.; Babadagi, E.; Savas, T.; Pekkan, E. GIS-Based Groundwater Potentiality Mapping Using AHP and FR Models in Central Antalya, Turkey. *Environ. Sci. Proc.* **2021**, *5*, 11. [[CrossRef](#)]
29. Muavhi, N.; Thamaga, K.H.; Mutoti, M.I. Mapping groundwater potential zones using relative frequency ratio, analytic hierarchy process and their hybrid models: Case of Nzhelele-Makhado area in South Africa. *Geocarto Int.* **2022**, *37*, 6311–6330. [[CrossRef](#)]
30. Ozdemir, A. GIS-based groundwater spring potential mapping in the Sultan Mountains (Konya, Turkey) using frequency ratio, weights of evidence and logistic regression methods and their comparison. *J. Hydrol.* **2011**, *411*, 290–308. [[CrossRef](#)]
31. Davoodi Moghaddam, D.; Rezaei, M.; Pourghasemi, H.R.; Pourtaghi, Z.S.; Pradhan, B. Groundwater spring potential mapping using bivariate statistical model and GIS in the Taleghan watershed Iran. *Arab. J. Geosci.* **2001**, *10* (Suppl. S2), S96–S101. [[CrossRef](#)]
32. Li, Y.; Abdelkareem, M.; Al-Arifi, N. Mapping Potential Water Resource Areas Using GIS-Based Frequency Ratio and Evidential Belief Function. *Water* **2023**, *15*, 480. [[CrossRef](#)]
33. Pradhan, B. Ground water potential zonation for basaltic watersheds using satellite remote sensing data and GIS techniques. *Cent. Eur. J. Geosci.* **2009**, *1*, 120–129.
34. Ayazi, M.H.; Pirasteh, S.; Arvin, A.K.P.; Pradhan, B.; Nikouravan, B.; Mansor, S. Disasters and risk reduction in groundwater: Zagros mountain southwest Iran using geo-informatics techniques. *Dis. Adv.* **2010**, *3*, 51–57.
35. Selvarani, A.G.; Maheswaran, G.; Elangovan, K. Identification of Artificial Recharge Sites for Noyyal River Basin Using GIS and Remote Sensing. *J. Indian Soc. Remote Sens.* **2017**, *45*, 67–77. [[CrossRef](#)]
36. Sahour, H.; Gholami, V.; Vazifedan, M.; Saeedi, S. Machine Learning Applications for Water-Induced Soil Erosion Modeling and Mapping. *Soil Tillage Res.* **2021**, *211*, 105032. [[CrossRef](#)]
37. Folharini, S.; Vieira, A.; Bento-Gonçalves, A.; Silva, S.; Marques, T.; Novais, J. Soil Erosion Quantification using Machine Learning in Sub-Watersheds of Northern Portugal. *Hydrology* **2023**, *10*, 7. [[CrossRef](#)]
38. Rahmati, O.; Melesse, A.M. Application of Dempster-Shafer theory, spatial analysis and remote sensing for groundwater potentiality and nitrate pollution analysis in the semi-arid region of Khuzestan, Iran. *Sci. Total Environ.* **2016**, *568*, 1110–1123. [[CrossRef](#)]
39. Al Saud, M. Mapping potential areas for groundwater storage in wadiaurnah basin, western Arabian peninsula, using remote sensing and geographic information system techniques. *Hydrogeol. J.* **2010**, *18*, 1481–1495. [[CrossRef](#)]
40. Ettazarini, S. Groundwater potential index: A strategically conceived tool for water research in fractured aquifers. *Environ. Geol.* **2007**, *52*, 477–487. [[CrossRef](#)]
41. Mukherjee, I.; Singh, U.K. Delineation of groundwater potential zones in a drought-prone semi-arid region of east India using GIS and analytical hierarchical process techniques. *Catena* **2020**, *194*, 104681. [[CrossRef](#)]
42. Villeneuve, S.; Cook, P.; Shanafield, M.; Wood, C.; White, N. Groundwater recharge via infiltration through an ephemeral riverbed, central Australia. *J. Arid. Environ.* **2015**, *117*, 47–58. [[CrossRef](#)]
43. Magesh, N.S.; Chandrasekar, N.; Soundranayagam, J.P. Delineation of groundwater potential zones in Theni district, Tamil Nadu, using remote sensing, GIS and MIF techniques. *Geosci. Front.* **2012**, *3*, 189–196. [[CrossRef](#)]
44. Shekhar, S.; Pandey, A.C. Delineation of groundwater potential zone in hard rock terrain of India using remote sensing, geographical information system (GIS) and analytic hierarchy process (AHP) techniques. *Geocarto Int.* **2014**, *30*, 402–421. [[CrossRef](#)]
45. Wang, X.; Zheng, W.; Tian, W.; Gao, Y.; Wang, X.; Tian, Y.; Li, J.; Zhang, X. Groundwater hydrogeochemical characterization and quality assessment based on integrated weight matter-element extension analysis in Ningxia, upper Yellow River, northwest China. *Ecol. Indic.* **2022**, *135*, 108525. [[CrossRef](#)]

46. Mi, L.; Tian, J.; Si, J.; Chen, Y.; Li, Y.; Wang, X. Evolution of groundwater in yinchuan oasis at the upper reaches of the yellow river after water-saving transformation and its driving factors. *Int. J. Environ. Res. Public Health* **2020**, *17*, 1304. [[CrossRef](#)]
47. Gao, X.; Wang, W.; Hou, B.; Gao, L.; Zhang, J.; Zhang, S.; Li, C.; Jiang, C. Analysis of karst groundwater pollution in northern China. *Carsologica Sinica*. **2020**, *39*, 287–289. [[CrossRef](#)]
48. O'Callaghan, J.F.; Mark, D.M. The extraction of drainage networks from digital elevation data. *Comput. Vis. Graph. Image Process.* **1984**, *28*, 323–344. [[CrossRef](#)]
49. Allafta, H.; Opp, C.; Patra, S. Identification of Groundwater Potential Zones Using Remote Sensing and GIS Techniques: A Case Study of the Shatt Al-Arab Basin. *Remote Sens.* **2021**, *13*, 112. [[CrossRef](#)]
50. Eastman, J.R.; Jin, W.; Kyem, A.K.P.; Toledano, J. Raster procedure for multi-criteria/multi-objective decisions. *Photogramm. Eng. Remote Sens.* **1995**, *61*, 539–547.
51. Pradhan, A.M.S.; Kim, Y.T. Relative effect method of landslide susceptibility zonation in weathered granite soil: A case study in Deokjeok-ri Creek, South Korea. *Nat. Hazards* **2014**, *72*, 1189–1217. [[CrossRef](#)]
52. Benjmel, K.; Amraoui, F.; Boutaleb, S.; Ouchchen, M.; Tahiri, A.; Touab, A. Mapping of groundwater potential zones in crystalline terrain using remote sensing, GIS techniques, and multicriteria data analysis (case of the Ighremregion, western Anti-Atlas, Morocco). *Water* **2020**, *12*, 471. [[CrossRef](#)]
53. Al-Djazouli, M.O.; Elmorabiti, K.; Rahimi, A.; Amellah, O. Fadil OAM.Delineating of groundwater potential zones based on remote sensing, GIS and analytical hierarchical process: A case of Waddai, eastern Chad. *Geojournal* **2020**, *86*, 1881–1894. [[CrossRef](#)]
54. Abdelkareem, M. Targeting flash flood potential areas using remotely sensed data and GIS techniques. *Nat. Hazards J.* **2017**, *85*, 19–37. [[CrossRef](#)]
55. Avand, M.; Janizadeh, S.; Tien Bui, D.; Pham, V.H.; Ngo, P.T.T.; Nhu, V.-H. A tree-based intelligence ensemble approach for spatial prediction of potential groundwater. *Int. J. Digital Earth* **2020**, *13*, 1408–1422. [[CrossRef](#)]
56. Lakshmi, S.; Reddy, Y. Identification of groundwater potential zones using GIS and remote sensing. *Int. J. Pure Appl. Math.* **2018**, *119*, 3195–3210.
57. Gebhardt, C.; Theis, S.E.; Paulat, M.; Ben-Bouallègue, Z. Uncertainties in COSMO-DE precipitation forecasts introduced by model perturbations and variation of lateral boundaries. *Atmos. Res.* **2011**, *100*, 168–177. [[CrossRef](#)]
58. Kanagaraj, G.; Suganthi, S.; Elango, L.; Magesh, N. Assessment of groundwater potential zones in Vellore district, Tamil Nadu, India using geospatial techniques. *Earth Sci. Inf.* **2019**, *12*, 211–223. [[CrossRef](#)]
59. Harini, P.; Sahadevan, D.K.; Das, I.C.; Manikyamba, C.; Durgaprasad, M.; Nandan, M.J. Regional groundwater assessment of Krishna RiverBasin using integrated GISapproach. *J. Indian Soc. Remote Sens.* **2018**, *46*, 1365–1377. [[CrossRef](#)]
60. Janizadeh, S.; Avand, M.; Jaafari, A.; Phong, T.V.; Bayat, M.; Ahmadisharaf, E.; Prakash, I.; Pham, B.T.; Lee, S. Prediction success of machine learning methods for flash flood susceptibility mapping in the tafresh watershed, Iran. *Sustainability* **2019**, *11*, 5426. [[CrossRef](#)]
61. Lee, S.; Pradhan, B. Probabilistic landslide hazards and risk mapping on Penang Island, Malaysia. *J. Earth Syst. Sci.* **2006**, *115*, 661–672. [[CrossRef](#)]
62. Dawood, F.; Akhtar, M.M.; Ehsan, M. Evaluating urbanization impact on stressed aquifer of Quetta Valley, Pakistan. *Desalination Water Treat.* **2021**, *222*, 103–113. [[CrossRef](#)]
63. Kalantar, B.; Al-Najjar HA, H.; Pradhan, B.; Saeidi, V.; Abdul Halin, A.; Ueda, N.; Naghibi, S.A. Optimized Conditioning Factors Using Machine Learning Techniques for Groundwater Potential Mapping. *Water* **2019**, *11*, 1909. [[CrossRef](#)]
64. Moghaddam, D.; Rahmati, O.; Haghizadeh, A.; Kalantari, Z. A Modeling Comparison of Groundwater Potential Mapping in a Mountain Bedrock Aquifer: QUEST, GARP, and RF Models. *Water* **2020**, *12*, 679. [[CrossRef](#)]
65. Anbazhagan, S.; Ramasamy, S.; Das Gupta, S. Remote sensing and GIS for artificial recharge study, runoff estimation and planning in Ayyar basin, Tamil Nadu, India. *Environ. Geol.* **2005**, *48*, 158–170. [[CrossRef](#)]
66. Opp, C. Bodenkörper. In *Geographie—Physische Geographie und Humangeographie*, 3rd ed.; Gebhardt, H., Glaser, R., Radtke, U., Reuber, P., Vött, A., Eds.; Springer: Berlin, Germany, 2011; pp. 485–490.
67. Achu, A.L.; Reghunath, R.; Thomas, J. Mapping of Groundwater Recharge Potential Zones and Identification of Suitable Site-Specific Recharge Mechanisms in a Tropical River Basin. *J. Earth Syst. Environ.* **2020**, *4*, 131–145. [[CrossRef](#)]
68. Berhanua, K.G.; Hatiye, S.D. Identification of Groundwater Potential Zones Using Proxy Data: Case study of Megech Watershed, Ethiopia Kibrit Gedam Berhanua, Samuel Dagalo Hatiye. *J. Hydroogy: Reg. Stud.* **2020**, *28*, 100676.
69. Gaur, S.; Chahar, B.R.; Grailot, D. Combined use of groundwater modeling and potential zone analysis for management of groundwater. *Int. J. Appl. Earth Obs. Geoinf.* **2011**, *13*, 127–139. [[CrossRef](#)]
70. Acharya, T.; Nag, S.K.; Basumallik, S. Hydraulic significance of fracture correlated lineaments in precambrian rocks in Purulia district, West Bengal. *J. Geol. Soc. India* **2012**, *80*, 723–730. [[CrossRef](#)]
71. Hossein, A.; Ardakani, H.; Ekhtesasi, M.R. Groundwater potentiality through Analytic Hierarchy Process (AHP) using remote sensing and Geographic Information System (GIS). *J. Geope* **2016**, *6*, 75–88.
72. Gannouni, S.; Gabtni, H. Structural interpretation of lineaments by satellite image processing (Landsat TM) in the region of Zahret Medien (Northern Tunisia). *J. Geogr. Inf. Syst.* **2015**, *7*, 119. [[CrossRef](#)]
73. Razavi-Termeh, S.V.; Sadeghi-Niaraki, A.; Choi, S. Groundwater Potential Mapping Using an Integrated Ensemble of Three Bivariate Statistical Models with Random Forest and Logistic Model Tree Models. *Water* **2019**, *11*, 1596. [[CrossRef](#)]

74. Alarifi, S.S.; Abdelkareem, M.; Abdalla, F.; Alotaibi, M. Flash Flood Hazard Mapping Using Remote Sensing and GIS Techniques in Southwestern Saudi Arabia. *Sustainability* **2022**, *14*, 14145. [[CrossRef](#)]
75. Abdekareem, M.; Al-Arifi, N.; Abdalla, F.; Mansour, A.; El-Baz, F. Fusion of Remote Sensing Data Using GIS-Based AHP-Weighted Overlay Techniques for Groundwater Sustainability in Arid Regions. *Sustainability* **2022**, *14*, 7871. [[CrossRef](#)]
76. Lentswe, G.B.; Lentswe, M. Delineation of potential groundwater recharge zones using analytic hierarchy 725 process-guided GIS in the semi-arid Motloutse watershed, eastern Botswana. *J. Hydrol. Reg. Stud.* **2020**, *28*, 100674. [[CrossRef](#)]
77. Pande, C.B.; Khadri, F.R.; Moharir, K.N.; Patode, R.S. Assessment of groundwater potential zonation of Mahesh 722 River basin Akola and Buldhana districts, Maharashtra, India using remote sensing and GIS techniques. *Sustain. Water Resour. Manag.* **2018**, *4*, 965–979. [[CrossRef](#)]
78. Abdelkareem, M.; Al-Arifi, N. The use of remotely sensed data to reveal geologic, structural, and hydrologic features and predict potential areas of water resources in arid regions. *Arab. J. Geosci.* **2021**, *14*, 1–15. [[CrossRef](#)]

Disclaimer/Publisher’s Note: The statements, opinions and data contained in all publications are solely those of the individual author(s) and contributor(s) and not of MDPI and/or the editor(s). MDPI and/or the editor(s) disclaim responsibility for any injury to people or property resulting from any ideas, methods, instructions or products referred to in the content.